The Fluxional Nature of the Hydrated Electron: Energy and Entropy Contributions to Aqueous Electron Free Energies

William J. Glover* and Benjamin J. Schwartz*

ACCESS | Metrics & More | Article Recommendations

ABSTRACT: There has been a great deal of recent controversy over the structure of the hydrated electron and whether it occupies a cavity or contains a significant number of interior waters (noncavity). The questions we address in this work are, from a free energy perspective, how different are these proposed structures? Do the different structures all lie along a single continuum, or are there significant differences (i.e., free energy barriers) between them? To address these questions, we have performed a series of one-electron calculations using umbrella sampling with quantum biased molecular dynamics along a coordinate that directly reflects the number of water molecules in the hydrated electron's interior. We verify that a standard cavity model of the hydrated electron behaves essentially as a hard sphere: the model is dominated by repulsion at short range such that water is expelled from a local volume around the electron, leading to a water solvation shell like that of a pseudohalide ion. The repulsion is much larger than thermal energies near room temperature, explaining why such models exhibit properties with little temperature dependence. On the other hand, our calculations reveal that a noncavity model is highly fluxional, meaning that thermal motions cause the number of interior waters to fluctuate from effectively zero (i.e., a cavity-type electron) to potentially above the bulk water density. The energetic contributions in the noncavity model are still repulsive in the sense that they favor cavity formation, so the fluctuations in structure are driven largely by entropy: the entropic cost for expelling water from a region of space is large enough that some water is still driven into the electron's interior. As the temperature is lowered and entropy becomes less important, the noncavity electron's structure is predicted to become more cavity-like, consistent with the observed temperature dependence of the hydrated electron's properties. Thus, we argue that although the specific noncavity model we study overestimates the preponderance of fluctuations involving interior water molecules, with appropriate refinements to correctly capture the true average number of interior waters and molar solvation volume, a fluxional model likely makes the most sense for understanding the various experimental properties of the hydrated electron.
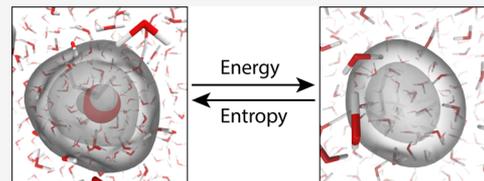
INTRODUCTION

Our understanding of the structure of the hydrated electron—an excess electron in liquid water—has been the subject of a great deal of controversy over the past few years.[1−10] The basic question is how the electron's wave function is distributed among the water molecules. Resonance Raman experiments show that the vibrational peaks associated with photoexcitation of the hydrated electron match well with those of bulk liquid water: Although its line shape is broadened and red-shifted, the O−H stretch lies roughly in the same place as that of bulk water, and the water bend is downshifted by only ∼1% in frequency.[11−14] This indicates that the influence of the electron on the bonding in water is largely perturbative and rules out models identifying the hydrated electron as a solvated water anion $H_2O^-_{(aq)}$. Instead, the excess electron's wave function is associated with several nearby but essentially intact water molecules.

Even with the knowledge that the hydrated electron has relatively little electronic overlap with any given nearby water molecule, we are still left with the question of the local molecular structure of the water associated with the excess electron. Early theories,[15] supported by mixed quantum/classical (MQC)

molecular dynamics (MD) simulations,[16] suggested that the hydrated electron occupies a cavity in the water, with a local hydration structure similar to that of chloride or bromide. In this picture, Pauli repulsion forces between the excess electron and the electrons in the occupied water MOs expel the water from the electron's location, so that the electron can be loosely thought of as a particle in a spherical box. A few years ago, however, we developed a new electron−water pseudopotential for describing the hydrated electron in MQC MD calculations and found that the resulting simulated hydrated electron displayed noncavity behavior:[1] instead of a cavity, the electronic wave function encompassed several water molecules, with electrostriction causing a slight enhancement of the interior water density relative to the surrounding bulk. Subsequently, QM/MM[17,18] and *ab initio* calculations[19−21] have supported a cavity picture; however, the radial distribution functions (RDF)

of QM/MM models display a more compact first solvation shell than the traditional one-electron models of Schnitker and Rossky (SR)[22] or Turi and Borgis (TB).[23] Only after incorporating multipole electrostatics, many-body polarization, and fitting to a Density Functional Theory (DFT) exchange-correlation potential does a MQC model[24] begin to approach the cavity size predicted by QM/MM. In addition, QM/MM models display a larger overlap of the excess electron's wave function with the first- and second-shell water molecules compared to the SR and TB models,[7] as much as ~50% overlap in the case of self-interaction-corrected DFT-based QM/MM simulations.[17]

The whole idea of having a significant number of water molecules inside the hydrated electron's wave function has been highly controversial.[1−10] In many of the MQC MD simulations that led to the cavity picture of the hydrated electron,[16,23] the pseudopotential employed was developed using the Phillips−Kleinman (PK) theory,[25] plus additional approximations or fitting strategies. In the PK theory, one can rigorously calculate a potential that contains the energetic penalty of enforcing the wave function of the excess electron to be orthogonal to the occupied molecular orbitals (MOs) of the water as determined via a Hartree−Fock (H−F) quantum chemistry calculation. The earliest electron−water potential developed with this formalism,[22] which predicted a cavity electron, turned out to contain an error.[26] Later work by Turi and Borgis (TB) led to a potential that also resulted in cavity formation for the hydrated electron (Figure 1, black solid curve).[23] The noncavity structure (Figure
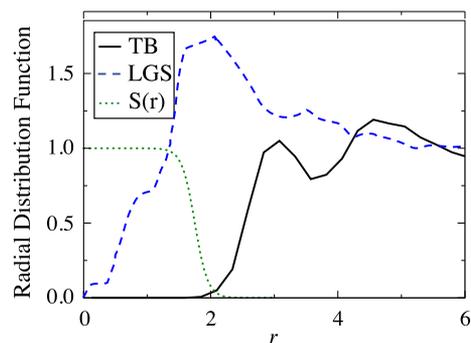

Figure 1. Hydrated electron center of mass:water oxygen radial distribution functions of competing models of the hydrated electron: LGS noncavity model (blue dashed curve) and TB cavity model (black solid curve). Also shown is the electron−water coordination number counting function, $S(r)$ (dotted green curve); by integrating $S(r)$ over the radial distribution functions (a coordinate we refer to as q^{cav}; see text for details), we see that on average, there are 0.85 water molecules "inside" the LGS electron and 0.0014 waters in the TB electron. In contrast, if we simply integrate the number of waters within 2.0 Å of each electron's center of mass without the $S(r)$ weighting function (a coordinate we refer to as N_W), we find 0.034 waters inside the TB electron and 1.48 waters in the LGS electron.

1, blue-dashed curve) from the potential we subsequently developed,[1] referred to as LGS in the literature, was based on an analytic reformulation of the PK theory,[27] which led to a numerically calculated potential that is identical to that presented by TB. The difference between our LGS potential and that previously presented by TB occurs primarily in the way the numerical potential was fit to an analytic function for use in molecular simulation, in addition to the use of a different polarization potential to describe electron−water correlation interactions.[2,7] It is mainly the differences in the PK fits that lead

to the dramatically different predicted structures for the TB and LGS hydrated electrons, as seen in Figure 1. Indeed Turi and Madarász pointed out that subtle changes in the LGS fit parameters can produce a potential that leads to a cavity-structure hydrated electron,[5] suggesting that there is a kind of structural phase transition that depends sensitively on the exact form of the potential, with the LGS potential lying very near to the transition point.[2] Similarly, when we reoptimized the TB polarization potential to better capture electron−water correlation effects at the CCSD(T) level of theory, we found that the reoptimized TB potential produces a noncavity electron with properties intermediate between the LGS and TB models.[28]

The best way to try to distinguish between different structural models of the hydrated electron is via their agreement (or lack thereof) with a variety of experimentally measured properties. Nearly every picture of the hydrated electron (cavity, noncavity, or intermediate) predicts optical absorption spectra that are in good agreement with experiments as long as they produce a ground-state excess electron with about the correct radius of gyration.[29] The absorption spectrum of the hydrated electron is known to redshift with increasing temperature at 1 atm pressure.[30−38] Both cavity and noncavity models capture some of this behavior, which results from the reduction in water density with increasing temperature.[39] However, as Bartels and co-workers showed, the dominant spectral redshift arises from a temperature-only effect (i.e., there is a redshift in the electron's absorption spectrum with temperature at *constant density*).[38] Cavity models completely miss this behavior,[28,39,40] while the LGS model reproduces this behavior, although the magnitude of the predicted redshift is about a factor of 2 exaggerated compared to experiments.[7,41,42]

Using an electrostatic field-frequency map parametrized to bulk water, the resonance Raman spectrum of the hydrated electron in the O−H stretch region is well reproduced by the LGS model, but not by the TB or other one-electron cavity models, which are blueshifted and narrowed compared to experiment.[7,41] However, very recent *ab initio* QM/MM calculations show that a cavity model can reproduce the experimental resonance Raman spectrum,[12] presumably due to a weakening of the O−H bonds via a small amount of σ^* occupation by the excess electron that is missed in the electrostatic field map.[43] Furthermore, a cavity model better reproduces the experimental resonance Raman spectrum of the hydrated electron in isotopic mixtures[13] than does the LGS model.[43]

Cavity model hydrated electrons are also predicted to display surface activity at the air/water interface,[44−46] whereas non-cavity electrons are strongly repelled from the interface.[28,46] Despite early claims,[47] liquid microjet photoelectron experiments show no evidence for a long-lived surface-bound hydrated electron species.[48,49] The persistence of Second Harmonic Generation (SHG) signals in one experiment does suggest that hydrated electrons can approach the surface.[50] However, the precise depth to which they approach is uncertain, and the authors could not rule out the SHG signal as arising from electrons even ~10 Å below the interface,[50] which we and others have argued do not count as surface species, since bulk-like behavior is obtained at this depth.[46,51]

Finally, the noncavity LGS model is able to quantitatively explain the experimentally measured decrease in the hydrated electron's excited-state lifetime with increasing temperature,[52] whereas the TB cavity model predicts no temperature

dependence to the excited-state lifetime.[36] The LGS noncavity electron model, however, predicts a negative molar solvation volume,[46] which is in contradiction with both experiment[53,54] and traditional cavity models.[46] Finally, the noncavity LGS model predicts time-resolved photoelectron experimental signals that match well with experiment,[55,56] whereas the TB cavity model predicts dynamic photoelectron spectroscopy features that are in qualitative disagreement with experiment.[57]

Despite the generally good agreement with many, but not all, experiments, there still has been significant controversy over the use of the LGS potential. For example, Herbert and Jacobson have shown that the hydrated electron's Vertical Binding Energies (VBE) computed for LGS configurations with Density Functional Theory (DFT)[3] and Hartree−Fock (H−F)[43] are a few eV less bound than the VBEs computed with the LGS potential and that the VBEs are also underbound compared to experiment. This suggests that the LGS electron is overly attracted to water, presumably as a result of inaccuracies in the analytic fit to the PK potential, a point we noted from early on.[2] As a result, it is likely that the LGS model overemphasizes the preponderance of structures involving water molecules internal to the electron, as would also be expected from the wrong sign of the predicted molar solvation volume. However, the agreement of the LGS model with the temperature dependence of the hydrated electron's properties, which we showed previously is connected to structural changes,[42] strongly suggests that the model is correctly capturing some essential physics missed by cavity models: the electron−water interaction should not be so strongly repulsive as to prevent temperature-dependent fluctuations of the water molecules internal to the electron.

The goal of the current paper is to understand how different models do or do not correctly predict the temperature dependence of the hydrated electron in more detail. To do this, we seek to compute the free energy differences between cavity and noncavity structures for both the TB cavity and LGS noncavity models and to understand the energetic and entropic contributions to these free energies. We accomplish this by taking advantage of a MQC MD formalism called Quantum Biased Molecular Dynamics (QBMD), which we recently developed, for umbrella sampling along a coordinate involving a quantum expectation value.[45] Our goal with this work is not to argue that one structure or the other is preferred; rather, our investigation is aimed at understanding what driving forces bring water into the interior of noncavity electrons and whether thermal fluctuations can cause cavity electrons to access noncavity-like structures or vice versa. In other words, the main question we address is whether or not the cavity and noncavity pictures of the hydrated electron are truly different or are better thought of as snapshots of a single entity spread along a structural continuum.

To achieve this goal, we start by creating a coordination number-based order parameter that allows us to cleanly classify hydrated electron structures along a cavity/noncavity continuum, and then we calculate Potentials of Mean Forces (PMFs) along this coordinate for both the TB cavity and LGS noncavity pseudopotentials in MQC MD simulations. We find that the TB hydrated electron behaves essentially like a hard sphere: There is a large free energy cost for placing water molecules in the electron's interior, leading to a structure so rigid that it is not surprising that the spectroscopy, and other properties of this object do not change with temperature at constant density. The LGS hydrated electron, in contrast, has a relatively flat free energy profile along our coordination-number order parameter,

indicating that the number of interior waters is highly fluxional at room temperature. The driving force behind these fluctuations is largely entropic: the internal energy contribution to the free energy favors cavity formation, but there is a large entropic penalty associated with excluding water from a significant volume in space to form a cavity. The balance between these competing energetics is what determines the LGS electron's average structure and also explains its temperature dependence: as T is lowered and entropy becomes less important, internal energy considerations drive the electron to become more cavity-like, leading to the observed blueshift in the absorption spectrum. Overall, we believe that although the LGS model does not perfectly capture the balance between the energetic and entropic contributions to the hydrated electron's structure, the correct structure must be characterized by some balance between these competing effects; cavity models with exaggerated repulsion terms that overwhelm the entropic penalty for cavity formation are missing an important part of the physics underlying the hydrated electron's structure.

■ THEORETICAL METHODS

A Cavity Order Parameter. In order to directly compare the free energies of cavity and noncavity hydrated electron models, we need to sample along a coordinate that connects cavity and noncavity structures. An idea for one such coordinate comes from examining the Radial Distribution Functions (RDF) in Figure 1: it is clear that in the TB cavity model the number of water molecules within ∼2 Å of the electron's center of mass is virtually zero, while for the LGS noncavity model there are a significant number of water molecules in this range. Therefore, a suitable order parameter is simply the total number of water molecules within a radius of about 2 Å from the electron's center, which we refer to as N_W. In order to be able to use such an order parameter in molecular dynamics simulations, however, it is better to find a collective coordinate that varies smoothly and continuously with particle position. Fortunately, continuous coordination number coordinates have been previously developed (albeit for purely classical simulations),[58] which we can adapt straightforwardly for use with our quantum biasing method.[45]

First, we define the cavity coordinate, q^{cav}, as a sum of "counting" functions, S, that gives the number of water molecules close to the electron:

$$q^{cav}(\boldsymbol{R}^N) = \sum_{i=1}^{N} S(|\boldsymbol{R}_i - \boldsymbol{r}_e|) \tag{1}$$

where $\boldsymbol{R}_i$ is the Cartesian position vector of the oxygen atom of water molecule i, $\boldsymbol{r}_e$ is the expectation value position of the electron (i.e., its center of mass), and the sum runs over all N classical water molecules in the simulation. The function $S(r)$ must be approximately equal to 1 for $r < r_c$ and 0 for $r > r_c$, where r_c is a cutoff radius beyond which water molecules are no longer considered to contribute to the coordination number of the electron for the purposes of distinguishing cavity from noncavity structures. We found that the Fermi function is a suitable choice for the counting function

$$S(r) = \frac{1}{\exp[\kappa(r - r_c)] + 1} \tag{2}$$

where κ governs how rapidly the function decays from 1 to 0. After some trial and error, we determined that values of $\kappa = 10$ Å^{-1} and $r_c = 1.75$ Å gave a cavity coordinate that clearly

identified the TB electron as a cavity and the LGS electron as noncavity, as indicated by their equilibrium average values of q^{cav} = 0.0014 ± 0.0001 and q^{cav} = 0.85 ± 0.02, respectively.

Once the umbrella-biased simulations in q^{cav} were run following the procedure described below, we also computed the discrete cavity order parameter, N_W, at each time step, and then generated a potential of mean force using indirect umbrella sampling according to eq 15 of ref 59.

Quantum Biased Molecular Dynamics (QBMD). The details of our QBMD method are presented elsewhere.[45] We briefly review the QBMD method here in order to better describe its application to biasing an electron cavity coordinate. Following the method of umbrella sampling,[59−61] one adds a harmonic biasing potential, U^{bias}, to the system's Hamiltonian that serves to restrain a collective coordinate, such as our cavity coordinate q^{cav}, close to a desired value, ζ

$$U^{bias} = \frac{1}{2}k(q^{cav}(\boldsymbol{R}^N) - \zeta)^2 \tag{3}$$

In order to propagate molecular dynamics in the presence of the restraining potential, we need to add biasing forces due to the gradients of eq 3

$$F_\alpha^{bias} = -k(q^{cav} - \zeta)\left[\frac{\partial q^{cav}}{\partial R_\alpha} + \nabla_{r_e}q^{cav}\cdot\frac{dr_e}{dR_\alpha}\right] \tag{4}$$

where α denotes a particular classical degree of freedom. The first term in the square bracket of eq 4 is the contribution to the gradient of the cavity coordinate from its explicit dependence on particle position and is trivially calculated from eqs 1 and 2. The second term in eq 4 results from the dependence of the cavity coordinate on the quantum expectation value position of the electron, which in turn depends on the positions of all the classical water molecules

$$\frac{dr_e}{dR_\alpha} = \frac{d}{dR_\alpha}\langle\psi|\hat{r}|\psi\rangle \tag{5}$$

where $\hat{r}$ is the quantum position operator and ψ is the electronic state, which is determined indirectly by the positions of the classical particles through the pseudopotential. We have shown previously that expectation value derivatives like the one in eq 5 can be calculated efficiently by solving a set of coupled-perturbed equations using Handy's and Schaefer's Z-vector trick.[62]

To generate potentials of mean force (PMFs) along the cavity coordinate, we used eight umbrella windows for the TB model centered on cavity coordinates ζ = i/6, where i = 0, 1, ...,7 is the umbrella window index. To ensure a good overlap of distributions of cavity coordinate between windows, we found it necessary to vary the spring constant depending on umbrella window index: for indices i = 0, 3, 4, ...,7, we set k = 3.6864 eV/Å². For index i = 1, we set k = 14.7456 eV/Å², and for index i = 2, we set k = 7.3728 eV/Å². For the LGS model, we used 10 umbrella windows centered on cavity coordinates ζ = i/4, where i = 0, 1, ...,9. The spring constant was set to k = 1.6384 eV/Å², except for window i = 9, where the spring constant was k = 3.2768 eV/Å². For TB, after a suitable period of equilibration, statistics were collected for each umbrella window over run lengths of between 700 and 850 ps. For LGS, after equilibration, each umbrella window was run for a length of between 320 and 440 ps. In order to calculate ensemble-averaged quantities, the samples from each umbrella window were combined and

reweighted using the multistate Bennett acceptance ratio method.[59]

Simulation Details. The details of the mixed/quantum classical simulation were chosen to follow closely our previous work on the hydrated electron.[1,7,28,42,45,57] The simulation cell was cubic with periodic boundary conditions and contained 499 SPC/Flex water molecules[63] at a fixed density of 0.9970479 g/cm³. The excess electron's wave function was represented on a compact Fourier grid that spanned a cubic box somewhat smaller than the full simulation cell. To avoid the electron's wave function from spilling onto the edge of the Fourier grid, the grid origin was recentered on the electron's center of mass every 10 fs in a manner described previously.[64] The size of the Fourier grid at convergence depended on which electron−water pseudopotential was used. For the LGS potential,[1] the Fourier grid comprised 32 points spanning 17.93 Å in each dimension, while the TB potential[23] allowed a smaller grid of 14 points spanning 15.68 Å. The electron's wave function and energy were found at each time step by solving the quantum eigenvalue problem with Davidson's algorithm.[65] Forces on the water molecules due to the electron were evaluated with the Hellman−Feynman theorem,[66,67] with the restraints included by adding in the biasing forces from eq 4. Classical dynamics was propagated with the velocity Verlet algorithm and a 0.5 fs time step, and the Canonical ensemble was sampled by rescaling velocities according to Bussi et al.'s method.[68]

■ RESULTS AND DISCUSSION

Figure 2 shows the calculated PMFs for the TB (panel a) and LGS (panel b) hydrated electron models as a function of q^{cav}. The data make clear that for the TB cavity electron, there is a substantial free energy penalty to insert any water within the central cavity. This means that the TB electron is effectively a hard sphere as far as the surrounding water is concerned. Thus, as a solute, the TB electron is essentially equivalent to a halide ion such as chloride or bromide, excluding the water from a significant local volume. In fact, the TB free energy curve is so steep compared to $k_B T$ that thermal excitation cannot change the TB electron's structure as far as the number of interior water molecules is concerned. Thus, the lack of temperature dependence of the TB (and other cavity[22,40]) electron's properties at constant density[39,41] can be readily explained by the fact that the TB electron's interaction with water is indeed hard-sphere-like, so that modest changes in absolute temperature (such as taking water from freezing to boiling) are small compared to the free energy required to change the local solvation structure.

In contrast, Figure 2 also shows that the LGS noncavity electron has a very different PMF, which is nearly flat along q^{cav}. The shallow free energy minimum has 1 water molecule occupying the interior of the electron's charge density, but interior water occupations of zero (i.e., a fully cavity structure) to nearly two waters are readily accessible, only requiring ≤2 $k_B T$ of thermal excitation, leading to an average occupation of 0.85 waters. Thus, the LGS electron has a highly fluxional structure at room temperature: even though the average interior water density is slightly enhanced,[1] at any given instant, the interior water density can range from essentially zero (i.e., cavity-like) to higher than that of bulk water. Thus, the PMFs in Figure 2 make clear that the TB and LGS models are not simply equivalent structures along a continuum but instead represent highly distinct structural entities: a hard-sphere-like rigid structure for
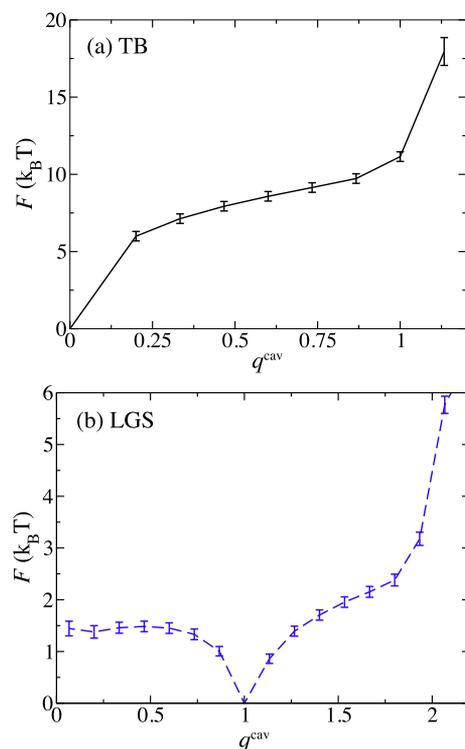
Figure 2. Potentials of mean force along the cavity coordinate, q^{cav} (eq 1) for the TB (panel a) and LGS (panel b) hydrated electron models. The PMFs show clearly that there is a large free energy penalty for having interior waters when using the TB cavity potential, which behaves essentially like a hard sphere. In contrast, the LGS hydrated electron accommodates a wide range of interior waters (from a full cavity to nearly 1.5 interior waters based on our choice of q^{cav}) with only a ~1.5 $k_B T$ free energy penalty at room temperature.

Figure 3. Free energy change as a function of the integer electron–water coordination number N_W (solid black curve) for the LGS model and its decomposition into internal energy (dashed blue curve) and entropy changes (dashed-dotted red curve). The zero of energy in each case is chosen as the zero-coordination number value. Also shown is the predicted free energy at 77 K (dotted green curve), calculated by scaling the room-temperature entropy contribution by 77/298.

the TB cavity electron and a porous, highly fluxional local structure for the LGS noncavity electron.

Given the PMFs in Figure 2, the next logical question to ask is why is the LGS electron's structure so fluxional along the cavity coordinate? To address this, we decomposed the free energy for the LGS electron into its internal energy (calculated directly as the ensemble averaged total energy in the simulation) and entropic (calculated as the difference between the free energy and internal energy) contributions. To reduce uncertainty errors, we used N_W, the simple integral of the number of water molecules within 2 Å of the electron's center of mass, as the cavity coordinate rather than the more complicated q^{cav}. The results are shown in Figure 3 as the blue-dashed curve for the LGS internal energy and red dotted-dashed curve for the LGS entropy. The data make clear that the LGS electron has an overall repulsive interaction energy with the local water: at room temperature, the energetic cost to place one water within 2 Å of the electron's center is ~7 $k_B T$, while that to place 2 waters near the electron's center is over 12 $k_B T$. Thus, despite complaints that the LGS potential overbinds the excess electron,[3−5,9,10,43] the data in Figure 2 make clear that the net energetic effect of forming the LGS noncavity structure is repulsive, consistent with Pauli exclusion forces keeping the excess electron away from the electrons occupying the closest water molecular orbitals. Thus, if internal energy were all that was important, the LGS electron would have a cavity structure that is a bit softer than but similar to that of the TB electron.
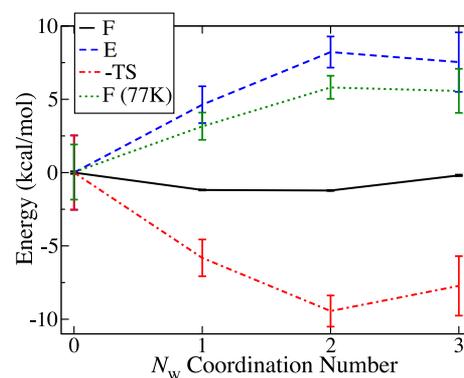
Given that the net interactions between the LGS electron and closest waters are repulsive, Figure 3 shows that the driving force to placing water into the electron's interior is entirely entropic in nature, which can be understood as an excluded volume effect. Indeed, the smallest possible entropic penalty would be for the water to simply ignore the presence of the excess electron and maintain its bulk structure, which is approximately the case at the equilibrium average interior occupation number of $N_W = 1.5$, or when the simulated temperature is ~350 K.[42] Of course, the electron is a charged object, so there also will be electrostrictive (i.e., ion−dipole attractive) forces that can both enhance the interior water density and potentially disrupt the local water H-bonding network, explaining why there is such a wide range of interior water densities that are entropically favorable. But overall, the entropy penalty for completely excluding water from the location of the electron is sufficiently high that the presence of at least some interior waters makes sense in the LGS model.

The fluxional structure of the LGS noncavity electron model can thus be explained by the fact that the magnitudes of the energetic and entropic terms are nearly equal and opposite, resulting in a free energy surface that is fairly flat along the N_W coordinate. This near balance of entropic and energetic terms also explains why the simulated LGS electron's structure is so sensitive to the details of the pseudopotential:[2,5] subtle changes in the pseudopotential that result in even a slight increase in the magnitude of the repulsion terms can tip the balance to an internal energy-dominated structure that prefers to have few or even no interior waters. This sensitivity does not exist for the TB electron since small changes in the shape of the potential do nothing to alter the fact that internal energy considerations remain entirely dominant and enforce a cavity structure. Only by including significant additional attraction at short range, such as was found necessary when reoptimizing the TB model to reproduce CCSD(T) interactions, can the TB model approach a noncavity picture of the hydrated electron.[28]

The fine balance between the energetic and entropic components for the noncavity LGS potential also explains the LGS electron's temperature dependence: as T drops and entropic contributions become less important, the LGS electron is predicted to adopt a more cavity-like structure, as we saw in previous work.[42] This change in structural character with T is driven home by the green dotted curve in Figure 3, which

presents an estimated PMF at liquid nitrogen temperatures (77 K), using the energetic contribution from the room temperature (298 K) simulations and scaling the entropic contribution by 77/298. At 77 K, the temperature is low enough that the internal energy dominates, leading to the prediction of a free energy minimum for a cavity-structure electron for the LGS model. The observation of such a low-temperature cavity structure is consistent with that observed in cryogenic pulse-radiolysis ESR experiments on the hydrated electron.[15] This suggests that the changes in absorption spectrum and other temperature-dependent properties of the hydrated electron are the result of a change in the number of waters fluctuating into the electron's interior as the bulk temperature is varied.[42]

Because the precise average structure of a noncavity electron will depend sensitively on the details of the entropic and energetic balance at a given temperature, there should be a spectrum of potentials that lead to fluxional behavior but with slightly different free energy balances and thus different temperature dependences. The LGS model represents one extreme of this spectrum, where the average structure is predominantly of noncavity nature. The LGS model predicts a negative molar solvation volume of the hydrated electron in disagreement with the positive experimental value,[53,54] which, together with the overestimation of temperature-dependent spectral shifts,[41] indicates that the entropic forces driving noncavity behavior have been overestimated (and/or the repulsive internal energetic contributions underestimated). On the other hand, the absence of temperature-dependent spectral shifts in the TB model[39] can be understood in the context of its lack of fluxional behavior, suggesting that the repulsive internal energetic contributions are too large relative to entropic forces in this model.

It is not yet clear where the various QM/MM and *ab initio* models of the hydrated electron[17−21] lie on the spectrum of fluxional behavior. Indeed, one of the goals of this work is to inspire future simulations of the hydrated electron to use our q^{cav} coordinate as a means to characterize the average structure and fluctuations of different hydrated electron models. The average structures for various *ab initio* models have been described as being cavity in nature,[17−21] as is evident in their RDFs, when reported.[18,69] However, in QM/MM DFT- (self-interaction corrected BLYP/molopt-TZV2P-GTH level)[17] and H−F-based simulations,[18] the first solvation shells are noticeably compacted compared to TB; the first maxima in the RDF occurring at 2.35 Å for the DFT simulations[17] and 2.5 Å for the H−F simulations[18] compared to 3.0 Å for the TB model.[23] Of further interest is the closest approach distance of the water oxygen to the electron's center of mass (i.e., the turn-on distance of the electron−oxygen RDF), r_{close}, which provides an estimate of the cavity size. The H−F-based QM/MM simulation has the same value as TB, $r_{close} = 1.8$ Å,[18,23] but the DFT-based QM/MM simulation has a smaller cavity, with a reported $r_{close} = 1.6$ Å.[17] A careful inspection of Figure 3 in ref 17 reveals that oxygen atoms actually approach as close as 1.4 Å to the electron's centroid position. Integrating the electron−oxygen RDF up to $r = 1.6$ Å gives an average population of 0.003 water molecules that are within the oxygen atom's van der Waals radius of the electron. Although this is a much smaller population than seen with LGS, it does suggest that this DFT-based QM/MM model exhibits fluxional behavior like LGS, but with the free energy minimum shifted to $q^{cav} = 0$, and with a free-energy penalty for noncavity formation that is intermediate to that of LGS and TB. Indeed, fluxional behavior in the *ab initio* calculations run to date may be

sufficiently rare that the limited sampling possible in such simulations (a few to at most tens of ps) does not adequately capture it.[70] The enhanced sampling procedures and q^{cav} coordinate proposed in this work could be applied to *ab initio* MD simulations in the future to address this issue.

■ CONCLUSIONS

In summary, using our recently developed QBMD method for quantum umbrella sampling,[45] we have explored the free energy properties of popular cavity and noncavity models of the hydrated electron as a function of the number of water molecules in the electron's interior. We find that the TB cavity model hydrated electron behaves effectively as a hard sphere, with a large free energy penalty for water molecules to occupy the ∼2.0 Å central cavity. The LGS noncavity model, on the other hand, is highly fluxional, with both cavity-like and high interior water density configurations accessible at room temperature, such that on average there is a slight interior density enhancement relative to the bulk. The fluxional nature of the LGS electron results from a near cancellation of the energetic and entropic contributions that determine the electron's structure, leading to a relatively flat PMF along the cavity coordinate: the LGS internal energy contributions are net repulsive, working to expel water from the electron's interior, whereas the entropic terms are effectively attractive, the result of an entropic penalty for excluding the water from a region of space. The energy/entropy balance is subtle enough that it is not surprising that small changes in the form of the LGS potential can alter this balance to produce hydrated electrons with different structures.[2,5] The vastly different free energy profiles indicate that the TB and LGS models are indeed structurally distinct, while the fluxional nature of LGS suggests that QM/MM and *ab initio* models[17−21] may fall along the same structural continuum as the LGS noncavity model but with an average interior density at lower values along the cavity coordinate.

Our free energy findings also can explain the temperature dependence of the different hydrated electron models. Cavity models show effectively no temperature dependence because their structure is determined by internal energy contributions that are sufficiently repulsive that modest temperature changes do nothing to affect the structural energy scale. In other words, in the TB model, repulsive interactions overwhelm entropic terms that we believe are important in determining the hydrated electron's structure, explaining why TB[39] (and other strongly repulsive cavity models[22,40]) entirely miss the known temperature dependence[37,41] of the hydrated electron's absorption spectrum at constant density. For the LGS model, on the other hand, reducing the temperature diminishes the entropic contributions to the free energy, so the electron's structure becomes more cavity-like as the internal energy begins to dominate; this is consistent with the cavity structure observed at the cryogenic temperatures in previous ESR experiments.[15] Our analysis also suggests that a slight change in the energy/entropy balance would strongly affect the predicted molar solvation volume of the hydrated electron, so that a structurally fluxional model is what would be needed to be consistent with both the temperature dependence and molar solvation volume experiments.

Overall, the fact that the LGS noncavity model overestimates the experimental temperature dependence of the hydrated electron's absorption spectrum[41] suggests that the energy/entropy balance for this model is somewhat off. However, our results strongly suggest that having some degree of balance,

meaning a fluxional model with water molecules that can occasionally enter the electron's interior with increasing propensity as the temperature is increased, is critical to explaining the known experimental properties of the hydrated electron. Work is underway to develop a one-electron MQC model that captures the right amount of fluxional behavior to give the correct temperature-dependent properties, while also having an average solvation structure that yields a molar solvation volume in agreement with experiment.

■ AUTHOR INFORMATION

Corresponding Authors

William J. Glover − *NYU Shanghai, Shanghai, China, NYU-ECNU Center for Computational Chemistry at NYU Shanghai, Shanghai, China, and New York University, New York, New York;* ⊙ orcid.org/0000-0002-2908-5680; Email: glover@nyu.edu

Benjamin J. Schwartz − *University of California, Los Angeles, Los Angeles, California;* ⊙ orcid.org/0000-0003-3257-9152; Email: schwartz@chem.ucla.edu

Complete contact information is available at:
https://pubs.acs.org/10.1021/acs.jctc.9b00496

Notes

The authors declare no competing financial interest.

■ ACKNOWLEDGMENTS

■ REFERENCES

(1) Larsen, R. E.; Glover, W. J.; Schwartz, B. J. Does the Hydrated Electron Occupy a Cavity? *Science* **2010**, *329*, 65.

(2) Larsen, R. E.; Glover, W. J.; Schwartz, B. J. Response to Comments on "Does the Hydrated Electron Occupy a Cavity?". *Science* **2011**, *331*, 1387.

(3) Herbert, J. M.; Jacobson, L. D. Structure of the Aqueous Electron: Assessment of One-Electron Pseudopotential Models in Comparison to Experimental Data and Time-Dependent Density Functional Theory. *J. Phys. Chem. A* **2011**, *115*, 14470.

(4) Jacobson, L. D.; Herbert, J. M. Comment on "Does the Hydrated Electron Occupy a Cavity?". *Science* **2011**, *331*, 1387.

(5) Turi, L.; Madarász, A. Comment on "Does the Hydrated Electron Occupy a Cavity?". *Science* **2011**, *331*, 1387.

(6) Turi, L.; Rossky, P. J. Theoretical Studies of Spectroscopy and Dynamics of Hydrated Electrons. *Chem. Rev.* **2012**, *112*, 5641.

(7) Casey, J. R.; Kahros, A.; Schwartz, B. J. To Be or Not to Be in a Cavity: The Hydrated Electron Dilemma. *J. Phys. Chem. B* **2013**, *117*, 14173.

(8) Turi, L. Hydrated Electrons in Water Clusters: Inside or Outside, Cavity or Noncavity? *J. Chem. Theory Comput.* **2015**, *11*, 1745.

(9) Herbert, J. M.; Coons, M. P. The Hydrated Electron. *Annu. Rev. Phys. Chem.* **2017**, *68*, 447.

(10) Herbert, J. M. Structure of the aqueous electron. *Phys. Chem. Chem. Phys.* **2019**, *21*, 20538.

(11) Tauber, M. J.; Mathies, R. A. Fluorescence and Resonance Raman Spectra of the Aqueous Solvated Electron. *J. Phys. Chem. A* **2001**, *105*, 10952.

(12) Tauber, M. J.; Mathies, R. A. Resonance Raman spectra and vibronic analysis of the aqueous solvated electron. *Chem. Phys. Lett.* **2002**, *354*, 518.

(13) Tauber, M. J.; Mathies, R. A. Structure of the Aqueous Solvated Electron from Resonance Raman Spectroscopy: Lessons from Isotopic Mixtures. *J. Am. Chem. Soc.* **2003**, *125*, 1394.

(14) Mizuno, M.; Tahara, T. Novel Resonance Raman Enhancement of Local Structure around Solvated Electrons in Water. *J. Phys. Chem. A* **2001**, *105*, 8823.

(15) Kevan, L. Solvated Electron Structure in Glassy Matrixes. *Acc. Chem. Res.* **1981**, *14*, 138.

(16) Rossky, P. J.; Schnitker, J. The Hydrated Electron: Quantum Simulation of Structure, Spectroscopy, and Dynamics. *J. Phys. Chem.* **1988**, *92*, 4277.

(17) Uhlig, F.; Marsalek, O.; Jungwirth, P. Unraveling the Complex Nature of the Hydrated Electron. *J. Phys. Chem. Lett.* **2012**, *3*, 3071.

(18) Holden, Z. C.; Rana, B.; Herbert, J. M. Analytic gradient for the QM/MM-Ewald method using charges derived from the electrostatic potential: Theory, implementation, and application to ab initio molecular dynamics simulation of the aqueous electron. *J. Chem. Phys.* **2019**, *150*, 144115.

(19) Kumar, A.; Walker, J. A.; Bartels, D. M.; Sevilla, M. D. A Simple ab Initio Model for the Hydrated Electron That Matches Experiment. *J. Phys. Chem. A* **2015**, *119*, 9148.

(20) Ambrosio, F.; Miceli, G.; Pasquarello, A. Electronic Levels of Excess Electrons in Liquid Water. *J. Phys. Chem. Lett.* **2017**, *8*, 2055.

(21) Wilhelm, J.; VandeVondele, J.; Rybkin, V. V. Dynamics of the Bulk Hydrated Electron from Many-Body Wave-Function Theory. *Angew. Chem., Int. Ed.* **2019**, *58*, 3890.

(22) Schnitker, J.; Rossky, P. J. An Electron−Water Pseudopotential for Condensed Phase Simulation. *J. Chem. Phys.* **1987**, *86*, 3462.

(23) Turi, L.; Borgis, D. Analytical Investigations of an Electron-Water Molecule Pseudopotential. II. Development of a New Pair Potential and Molecular Dynamics Simulations. *J. Chem. Phys.* **2002**, *117*, 6186.

(24) Jacobson, L. D.; Herbert, J. M. A One-Electron Model for the Aqueous Electron that Includes Many-Body Electron-Water Polarization: Bulk Equilibrium Structure, Vertical Electron Binding Energy, and Optical Absorption Spectrum. *J. Chem. Phys.* **2010**, *133*, 154506.

(25) Szász, L. *Pseudopotential Theory of Atoms and Molecules*; J. Wiley, 1985.

(26) Larsen, R. E.; Glover, W. J.; Schwartz, B. J. Comment on "An electron-water pseudopotential for condensed phase simulation" [J. Chem. Phys. 86, 3462 (1987)]. *J. Chem. Phys.* **2009**, *131*, No. 037101.

(27) Smallwood, C. J.; Larsen, R. E.; Glover, W. J.; Schwartz, B. J. A Computationally Efficient Exact Pseudopotential Method. I. Analytic Reformulation of the Phillips-Kleinman Theory. *J. Chem. Phys.* **2006**, *125*, No. 074102.

(28) Glover, W. J.; Schwartz, B. J. Short-Range Electron Correlation Stabilizes Noncavity Solvation of the Hydrated Electron. *J. Chem. Theory Comput.* **2016**, *12*, 5117.

(29) Bartels, D. M. Moment analysis of hydrated electron cluster spectra: Surface or internal states? *J. Chem. Phys.* **2001**, *115*, 4404.

(30) Gottschall, W. C.; Hart, E. J. The effect of temperature on the absorption spectrum of the hydrated electron and on its bimolecular recombination reaction. *J. Phys. Chem.* **1967**, *71*, 2102.

(31) Hart, E. J.; Michael, B. D.; Schmidt, K. H. Absorption spectrum of eaq- in the temperature range −4 to 390.deg. *J. Phys. Chem.* **1971**, *75*, 2798.

(32) Dixon, R. S.; Lopata, V. J. Spectrum of the solvated electron in heavy water up to 445 K. *Radiat. Phys. Chem.* **1978**, *11*, 135.

(33) Jou, F.-Y.; Freeman, G. R. Band resolution of optical spectra of solvated electrons in water, alcohols, and tetrahydrofuran. *Can. J. Chem.* **1979**, *57*, 591.

(34) Jou, F.-Y.; Freeman, G. R. Temperature and isotope effects on the shape of the optical absorption spectrum of solvated electrons in water. *J. Phys. Chem.* **1979**, *83*, 2383.

(35) Tuttle, T. R.; Golden, S. Shape stability of solvated-electron optical absorption bands. Part 1.—Experimental basis. *J. Chem. Soc., Faraday Trans. 2* **1981**, *77*, 873.

Journal of Chemical Theory and Computation
pubs.acs.org/JCTC
Article

(36) Christensen, H.; Sehested, K. The hydrated electron and its reactions at high temperatures. *J. Phys. Chem.* **1986**, *90*, 186.

(37) Bartels, D. M.; Takahashi, K.; Cline, J. A.; Marin, T. W.; Jonah, C. D. Pulse Radiolysis of Supercritical Water. 3. Spectrum and Thermodynamics of the Hydrated Electron. *J. Phys. Chem. A* **2005**, *109*, 1299.

(38) Du, Y.; Price, E.; Bartels, D. M. Solvated Electron Spectrum in Supercooled Water and Ice. *Chem. Phys. Lett.* **2007**, *438*, 234.

(39) Nicolas, C.; Boutin, A.; Lévy, B.; Borgis, D. Molecular simulation of a hydrated electron at different thermodynamic state points. *J. Chem. Phys.* **2003**, *118*, 9689.

(40) Wallqvist, A.; Martyna, G.; Berne, B. J. Behavior of the hydrated electron at different temperatures: structure and absorption spectrum. *J. Phys. Chem.* **1988**, *92*, 1721.

(41) Casey, J. R.; Larsen, R. E.; Schwartz, B. J. Resonance Raman and Temperature-Dependent Electronic Absorption Spectra of Cavity and Noncavity Models of the Hydrated Electron. *Proc. Natl. Acad. Sci. U. S. A.* **2013**, *110*, 2712.

(42) Zho, C. C.; Farr, E. P.; Glover, W. J.; Schwartz, B. J. Temperature dependence of the hydrated electron's excited-state relaxation. I. Simulation predictions of resonance Raman and pump-probe transient absorption spectra of cavity and non-cavity models. *J. Chem. Phys.* **2017**, *147*, No. 074503.

(43) Dasgupta, S.; Rana, B.; Herbert, J. M. Ab Initio Investigation of the Resonance Raman Spectrum of the Hydrated Electron. *J. Phys. Chem. B* **2019**, *123*, 8074.

(44) Madarász, Á.; Rossky, P. J.; Turi, L. Excess Electron Relaxation Dynamics at Water/Air Interfaces. *J. Chem. Phys.* **2007**, *126*, 234707.

(45) Glover, W. J.; Casey, J. R.; Schwartz, B. J. Free Energies of Quantum Particles: The Coupled-Perturbed Quantum Umbrella Sampling Method. *J. Chem. Theory Comput.* **2014**, *10*, 4661.

(46) Casey, J. R.; Schwartz, B. J.; Glover, W. J. Free Energies of Cavity and Noncavity Hydrated Electrons Near the Instantaneous Air/Water Interface. *J. Phys. Chem. Lett.* **2016**, *7*, 3192.

(47) Siefermann, K. R.; Liu, Y.; Lugovoy, E.; Link, O.; Faubel, M.; Buck, U.; Winter, B.; Abel, B. Binding Energies, Lifetimes and Implications of Bulk and Interface Solvated Electrons in Water. *Nat. Chem.* **2010**, *2*, 274.

(48) Lubcke, A.; Buchner, F.; Heine, N.; Hertel, I. V.; Schultz, T. Time-Resolved Photoelectron Spectroscopy of Solvated Electrons in Aqueous NaI Solution. *Phys. Chem. Chem. Phys.* **2010**, *12*, 14629.

(49) Buchner, F.; Schultz, T.; Lubcke, A. Solvated Electrons at the Water-Air Interface: Surface Versus Bulk Signal in Low Kinetic Energy Photoelectron Spectroscopy. *Phys. Chem. Chem. Phys.* **2012**, *14*, 5837.

(50) Sagar, D. M.; Bain, C. D.; Verlet, J. R. R. Hydrated Electrons at the Water/Air Interface. *J. Am. Chem. Soc.* **2010**, *132*, 6917.

(51) Coons, M. P.; You, Z.-Q.; Herbert, J. M. The Hydrated Electron at the Surface of Neat Liquid Water Appears To Be Indistinguishable from the Bulk Species. *J. Am. Chem. Soc.* **2016**, *138*, 10879.

(52) Farr, E. P.; Zho, C.-C.; Challa, J. R.; Schwartz, B. J. Temperature dependence of the hydrated electron's excited-state relaxation. II. Elucidating the relaxation mechanism through ultrafast transient absorption and stimulated emission spectroscopy. *J. Chem. Phys.* **2017**, *147*, No. 074504.

(53) Borsarelli, C. D.; Bertolotti, S. G.; Previtali, C. M. Thermodynamic Changes Associated with the Formation of the Hydrated Electron after Photoionization of Inorganic Anions: a Time-Resolved Photoacoustic Study. *Photochem. Photobiol. Sci.* **2003**, *2*, 791.

(54) Janik, I.; Lisovskaya, A.; Bartels, D. M. Partial Molar Volume of the Hydrated Electron. *J. Phys. Chem. Lett.* **2019**, *10*, 2220.

(55) Elkins, M. H.; Williams, H. L.; Shreve, A. T.; Neumark, D. M. Relaxation Mechanism of the Hydrated Electron. *Science* **2013**, *342*, 1496.

(56) Karashima, S.; Yamamoto, Y.-i.; Suzuki, T. Resolving Non-adiabatic Dynamics of Hydrated Electrons Using Ultrafast Photoemission Anisotropy. *Phys. Rev. Lett.* **2016**, *116*, 137601.

(57) Zho, C.-C.; Schwartz, B. J. Time-Resolved Photoelectron Spectroscopy of the Hydrated Electron: Comparing Cavity and Noncavity Models to Experiment. *J. Phys. Chem. B* **2016**, *120*, 12604.

(58) Patel, A. J.; Varilly, P.; Chandler, D.; Garde, S. Quantifying Density Fluctuations in Volumes of All Shapes and Sizes Using Indirect Umbrella Sampling. *J. Stat. Phys.* **2011**, *145*, 265.

(59) Shirts, M. R.; Chodera, J. D. Statistically Optimal Analysis of Samples from Multiple Equilibrium States. *J. Chem. Phys.* **2008**, *129*, 124105.

(60) Torrie, G. M.; Valleau, J. P. Nonphysical sampling distributions in Monte Carlo free-energy estimation: Umbrella sampling. *J. Comput. Phys.* **1977**, *23*, 187.

(61) Kästner, J. Umbrella sampling. *WIREs Comput. Mol. Sci.* **2011**, *1*, 932.

(62) Handy, N. C.; Schaefer, H. F. On the evaluation of analytic energy derivatives for correlated wave functions. *J. Chem. Phys.* **1984**, *81*, 5031.

(63) Toukan, K.; Rahman, A. Molecular-Dynamics Study of Atomic Motions in Water. *Phys. Rev. B: Condens. Matter Mater. Phys.* **1985**, *31*, 2643.

(64) Glover, W. J.; Larsen, R. E.; Schwartz, B. J. The roles of electronic exchange and correlation in charge-transfer-to-solvent dynamics: Many-electron nonadiabatic mixed quantum/classical simulations of photoexcited sodium anions in the condensed phase. *J. Chem. Phys.* **2008**, *129*, 164505.

(65) Davidson, E. R. The Iterative Calculation of a Few of the Lowest Eigenvalues and Corresponding Eigenvectors of Large Real-Symmetric Matrices. *J. Comput. Phys.* **1975**, *17*, 87.

(66) Hellmann, H. *Einführung in die Quantenchemie*; F. Deuticke: Leipzig, 1937.

(67) Feynman, R. P. Forces in Molecules. *Phys. Rev.* **1939**, *56*, 340.

(68) Bussi, G.; Donadio, D.; Parrinello, M. Canonical Sampling Through Velocity Rescaling. *J. Chem. Phys.* **2007**, *126*, No. 014101.

(69) Uhlig, F.; Marsalek, O.; Jungwirth, P. Electron at the Surface of Water: Dehydrated or Not? *J. Phys. Chem. Lett.* **2013**, *4*, 338.

(70) For example, if the free energy of a noncavity fluctuation were 6 k_BT higher than cavity structures (approximately halfway between that of LGS and TB), then noncavity structures would be observed only ~0.3% of the time, or just 30 time steps out of a 10-ps simulation, which could easily be missed over if not every MD snapshot is saved and analyzed.